Seismic evidence for a slab tear at the Puerto Rico Trench

Hallie E. Meighan,[1] Jay Pulliam,[1] Uri ten Brink,[2] and Alberto M. López-Venegas[3]

Received 12 November 2012; revised 17 May 2013; accepted 20 May 2013.

[1] The fore-arc region of the northeast Caribbean plate north of Puerto Rico and the Virgin Islands has been the site of numerous seismic swarms since at least 1976. A 6 month deployment of five ocean bottom seismographs recorded two such tightly clustered swarms, along with additional events. Joint analyses of the ocean bottom seismographs and land-based seismic data reveal that the swarms are located at depths of 50–150 km. Focal mechanism solutions, found by jointly fitting *P* wave first-motion polarities and *S*/*P* amplitude ratios, indicate that the broadly distributed events outside the swarm generally have strike- and dip-slip mechanisms at depths of 50–100 km, while events at depths of 100–150 km have oblique mechanisms. A stress inversion reveals two distinct stress regimes: The slab segment east of 65°W longitude is dominated by trench-normal tensile stresses at shallower depths (50–100 km) and by trench-parallel tensile stresses at deeper depths (100–150 km), whereas the slab segment west of 65°W longitude has tensile stresses that are consistently trench normal throughout the depth range at which events were observed (50–100 km). The simple stress pattern in the western segment implies relatively straightforward subduction of an unimpeded slab, while the stress pattern observed in the eastern segment, shallow trench-normal tension and deeper trench-normal compression, is consistent with flexure of the slab due to rollback. These results support the hypothesis that the subducting North American plate is tearing at or near these swarms. The 35 year record of seismic swarms at this location and the recent increase in seismicity suggest that the tear is still propagating.

Citation: Meighan, H. E., J. Pulliam, U. ten Brink, and A. M. López-Venegas (2013), Seismic evidence for a slab tear at the Puerto Rico Trench, *J. Geophys. Res. Solid Earth*, *118*, doi:10.1002/jgrb.50227.

1. Introduction

[2] The northeast Caribbean displays a variety of complex tectonic interactions and a high rate of seismicity [*Engdahl et al*., 1998; *Mann et al*., 2002]. Earthquake swarms, clusters of seismic events that occur in a time span of hours or days without a distinct main shock [*Roland and McGuire*, 2009], have been determined by analysts, based on recordings by land-based stations, to have occurred frequently off the northeastern coast of Puerto Rico during the last 35 years [*Pulliam et al*., 2007]. Accuracy of these event locations is related directly to the azimuthal distribution of recorded seismic observations. Permanent stations are located only on islands, which creates unavoidable bias in hypocenter locations due to limited azimuthal coverage and the lateral heterogeneity of the subduction zone in which the events typically occur. This limitation can be overcome temporarily by deployments of ocean bottom seismographs (OBSs) in locations seaward of the seismogenic zones; such deployments can be especially helpful if they capture one or more earthquake swarms. This study reports on stress patterns in the northeast Caribbean deduced from two swarms, plus additional events, that were recorded by a joint OBS and land-based seismic network.

[3] The tectonic setting in this region transitions from true dip-slip subduction of the North American (NOAM) plate beneath the Caribbean (CAR) plate along the Lesser Antilles Volcanic Arc, to a transform regime west of Puerto Rico (Figure 1). Obli`que subduction of the NOAM plate (recently determined to occur at 20 mm/yr at an azimuth of 254° by *DeMets et al*. [2010]) dominates in the vicinity of Puerto Rico and the U.S. and British Virgin Islands. In this location, the plate margin is concave in shape, which creates geometric complications as the downgoing NOAM slab is forced around the high-curvature margin [*ten Brink*, 2005; *Mann et al*., 2002]. This subduction geometry is likely accommodated by a shear zone or tear within the slab, of which the tearing process could produce earthquake swarms [*ten Brink*, 2005]. Slab tears have been identified in other tectonically similar regions as well [*Bautista et al*., 2001; *Clark et al*., 2008; *Govers and Wortel*, 2005; *Millen and Hamburger*, 1998; *Miller et al*., 2006; *Rosenbaum et al*., 2008].

Additional supporting information may be found in the online version of this article

[1]Geology Department, Baylor University, Waco, Texas, USA.
[2]Woods Hole Science Center, USGS, Woods Hole, Massachusetts, USA.
[3]Geology Department, University of Puerto Rico, Mayagüez, Puerto Rico.

Corresponding author: H. E. Meighan, Geology Department, Baylor University, One Bear Pl. 97354, Waco, TX 76798, USA. (hallie_meighan@baylor.edu)

2169-9313/13/10.1002/jgrb.50227

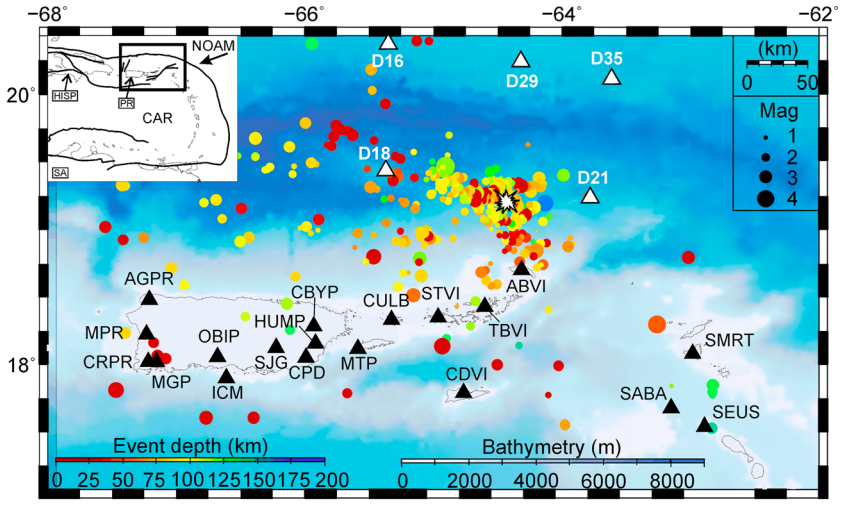

Figure 1. Major plate boundaries, major continents, and islands are outlined and labeled by solid black lines, solid arrow is relative plate motion vector [*DeMets et al*., 2010], and black box indicates area of zoomed-in large bathymetric map (Caribbean inset map). Filled triangles represent locations of seismograph stations used in this study with corresponding names (black are affiliated with regional seismic networks; white are from this OBS deployment), filled circles represent earthquake focii from our data set (color scaled by focal depth), and June swarm location denoted by white star (bathymetric, station, and event map of the NE Caribbean). Five stations (D16, D18, D21, D29, and D35) located in and around the trench are from the 6 month ocean bottom seismograph (OBS) array deployment and increased azimuthal coverage of the land-based stations. Events were located using the joint OBS-PRSN data set, which provided better constraints due to the good azimuthal coverage of observations. A Wadati-Benioff Zone is not clearly observed within this data set. NOAM, North American plate; CAR, Caribbean plate; PR, Puerto Rico; HISP, Hispaniola; SA, South America.

[4] The Wadati-Benioff zone of the subducting NOAM slab has been observed by *Fischer and McCann* [1984], *Engdahl et al*. [1998], and observed more recently using events from the regional Puerto Rico Seismic Network earthquake database. The maximum depth of the plate has been interpreted from relocated earthquake hypocenters to be 150 km [*ten Brink*, 2005]. The Wadati-Benioff zone has a 20° dip along the northern boundary of the Puerto Rico Trench, with a sudden 5° dip decrease off the NE coast of Puerto Rico, at approximately 64.5°W [*ten Brink*, 2005]. This is also the location of the recorded seismic swarms and where a slab tear has been proposed to be actively propagating, based on the bathymetry, gravity, seismicity, stress changes related to the subduction of a seamount, timing of the trench collapse, seismic anisotropy, and continuous GPS vector analyses [*ten Brink and López-Venegas*, 2012; *ten Brink*, 2005; *Meighan and Pulliam*, 2013]. Clear understanding of the geometry and mechanisms within the subducting slab depends on the accuracy of the earthquake hypocenters. Temporary deployments of OBS have been shown to resolve the location bias of land-based seismographic networks in submarine-dominated tectonic settings, such as the southern Tyrrhenian Sea, Taiwan, southern New Hebrides arc, central Aleutian subduction zone, South Shetland Islands, offshore Japan, northern Ecuador, and the East Pacific Rise [*Barberi et al*., 2006; *Begnaud et al*., 2000; *Chang et al*., 2008; *Coudert et al*., 1981; *Dahm*, 2006; *Frohlich et al*., 1982; *Maurice et al*., 2003; *Montagner et al*., 1994; *Nishizawa et al*., 1992; *Pontoise and Monfret*, 2004; *Pulliam et al*., 2003; *Shen et al*., 1997; *Webb*, 1998].

[5] This study focuses on the characterization of local tectonics by combining seismic observations from 6 month, continuously recording OBS and from land-based island stations. From March to September 2007, five OBSs were positioned in and around the region of most frequent previous swarms (Figure 1). The combined Puerto Rico Seismic Network (PRSN) and OBS data set captured approximately 600 events in addition to improving hypocenter constraints with the increased station distribution. The focal mechanism solutions of these events and the stress field in which they occurred were examined in order to understand their relationship with the proposed shear zone or slab tear.

2. Data

[6] Fifteen seismic stations operated by the Puerto Rico Seismic Network (PRSN) and five OBSs from the Woods Hole Oceanographic Institution (WHOI) were used in this study (Table S1 in the supporting information and Figure 1). Each short-period OBS contained a three-component Geospace GS-11D geophone (two horizontal and one vertical component), a hydrophone, and a Quanterra 330 digitizer/recorder. The OBS deployed the geophone in an external package by means of a fiberglass arm, but did not have a way to determine azimuthal orientation of the two horizontal components once it had reached the seafloor. One option for determining the orientation of horizontal components is to shoot an air gun in a pattern around the OBS and compute geophone orientation from the relative arrival times of subsequent water waves. However, this was not done for this deployment, and as such, the

orientation of horizontal components was not determined. The Quanterra 330s were programmed to record the geophones' data streams at 100 samples/s; clock drifts were determined and corrected by WHOI Ocean Bottom Seismograph Instrument Pool personnel. The glass spheres used by these OBSs have a depth rating of 6.5 km, so precise placement of the instruments was crucial in and around the Puerto Rico Trench, where depths reach 8.3 km. Three of the OBS stations (D16, D29, and D35) were deployed along the northern edge of the Puerto Rico Trench, station D21 was deployed at the southern edge of the Puerto Rico Trench, and station D18 was dropped directly on the Main Ridge Seamount within the trench (Figure 1).

[7] Several factors were taken into account when jointly processing the land-based observations and those from the OBS. The seafloor noise spectrum contains a higher level of background noise with frequencies less than 0.1 Hz than that of land stations [*Pulliam et al*., 2003]. Coupling between the OBS instrumentation and unconsolidated seafloor sediment can be weak at some OBS sites, which makes it difficult to identify seismic phases and can lead to "ringing" (fairly monochromatic signals). Lastly, amplitudes are often attenuated at higher frequencies compared to land-based observations of the same signals, rendering *P* and *S* arrivals more emergent than impulsive, and therefore more difficult to pick accurately.

[8] The land- and seafloor-based seismic observations were compiled into an Antelope database for preprocessing, as described below. ("Antelope" is a commercial seismic analysis package developed by Boulder Real Time Technologies.) Many of the phase arrivals recorded by PRSN stations within our data set had already been picked and their associated events located by analysts at the PRSN, as part of routine monitoring (see also *Clinton et al*. [2006] for more information regarding the PRSN). Nevertheless, every arrival pick that was used in the analysis was examined and manually adjusted. The picked phase arrivals were associated to corresponding events, *P* and *S* wave amplitudes were measured, first-motion *P* wave polarities were detected, and preliminary hypocenter locations using the *iasp91* 1-D velocity model were calculated [*Kennett and Engdahl*, 1991]. All operations that were performed automatically were checked manually. Waveforms that exhibited high levels of seismic noise or abnormal damping were excluded from further location processing because arrivals were indistinguishable from the background noise.

3. Seismic Analysis

[9] Details of the event location procedure, including the application of relative relocation algorithms, are the subject of a companion paper (A. M. López-Venegas et al., manuscript in preparation, 2013); only the characteristics of the absolute event locations that are relevant for this study of stress patterns will be summarized here. Events recorded during the 6 month deployment (average magnitude of 2.9) were relocated using the NonLinLoc software package [*Lomax et al*., 2000]. This program uses nonlinear, global-search algorithms for the probabilistic search of earthquakes within 3-D Earth models to find the minimum-residual solution [*Lomax et al*., 2000]. NonLinLoc algorithms follow the methods of *Tarantola and Valette*'s [1982] probabilistic inversion and the shortest-path method of traveltime computation in heterogeneous media [*Moser et al*., 1992; *Wittlinger et al*., 1993].

[10] The recorded data set has approximately 600 events, spanning depths from 0 to 200 km and with local magnitudes <4. Depth constraints are discussed further in the previously mentioned companion paper (A. M. López-Venegas et al., manuscript in preparation, 2013). Two seismic swarms occurred during the March–September 2007 OBS deployment. The first was from 16 to 18 April (approximately 40 events) and the second occurred from 24 to 26 June (approximately 180 events), with local magnitudes ranging from 1.7 to 3.7 (derived using the "dbml" Antelope tool). Both of these swarms were located offshore in an area that was surrounded by the OBS, providing good azimuthal constraints for the location; however, the hypocenters do not define a clear Wadati-Benioff zone. In addition, the large swarm on 24–26 June was centered at approximately 19.2°N, 64.5°W (swarm location denoted by star in Figure 1) and spanned depths of approximately 50–90 km.

4. Focal Mechanism Solutions

[11] Accurate fault plane solutions for small-magnitude earthquakes require a station distribution with small gaps in azimuth, a well-defined velocity model, and *P* wave first-arrival polarities. Where station distribution is poor, sampling of the focal sphere is incomplete; therefore, the addition of *S*/*P* amplitude ratios can supplement the first-arrival information [*Hardebeck and Shearer*, 2002, 2003; *Julian and Foulger*, 1996; *Kisslinger*, 1980; *Snoke et al*., 1984]. Including these ratios in focal mechanism calculations has also proved successful in regions with limited data coverage and/or events of small magnitude, such as the Alpine Fault in New Zealand, offshore SW Taiwan, Atotsugawa Fault in central Japan, Southern California, São Miguel Island, and western Skagerrak [*Boese et al*., 2012; *Chang et al*., 2008; *Imanishi et al*., 2011; *Kilb and Hardebeck*, 2006; *Silva et al*., 2012; *Sørensen et al*., 2011; *Yang et al*., 2012].

[12] Advantages of using *S*/*P* amplitude ratios include the following: (1) The observation location on the focal sphere is more accurately constrained, (2) the number of observations per event increases, and (3) the ratio values increase with increased proximity to nodal planes [*Hardebeck and Shearer*, 2002, 2003; *Julian and Foulger*, 1996; *Kisslinger*, 1980; *Snoke et al*., 1984; *Yang et al*., 2012]. At a given station, there are several factors that contribute to the observed amplitude; however, using the *S*/*P* ratio generally reduces the need for amplitude corrections [*Hardebeck and Shearer*, 2002]. In regions where a comprehensive sampling of azimuths with which to constrain the positions of nodal planes is not available, the incorporation of amplitude ratios is critical, as they reach their maxima along nodal planes.

[13] The HASH software package combines first-motion polarity picks with associated *S*/*P* amplitude ratios, accounts for errors in both hypocenter locations and seismic velocity models, and returns the best fit solution with associated errors [*Kraft et al*., 2006; *Silva et al*., 2012]. HASH generates a set of mechanisms for each event by incorporating the *S*/*P* observation uncertainty into the inversion; the average of the set is the preferred mechanism as long as it meets requirements prescribed by the user and the program [*Hardebeck and*

Shearer, 2002, 2003]. Imposing this requirement removed 9% of the events from this data set, which generated a total of 545 focal mechanism solutions. Solution uncertainties are estimated from the span of acceptable solutions and a quality flag (A-D) is assigned. "Quality" of mechanisms is determined using the parameters suggested in a recent study by *Yang et al*. [2012], in which ~200,000 focal mechanisms were recorded by a dense seismic network in Southern California to determine the relationships between fault plane uncertainties and 12 other parameters.

[14] Solution quality was based upon the azimuthal gap between two neighboring stations on the focal sphere, fault plane uncertainties (FPU; the root mean square angular difference in acceptable solutions), probability that acceptable solutions are close to the preferred solution (PROB), and how well the stations sample the focal sphere. The minimum azimuthal gap requirement for A-quality mechanisms was loosened to $<170°$, equivalent to the B-C quality rating from *Yang et al*. [2012], because the set of seismographic stations (including OBS) do not provide a comprehensive sampling of azimuths from offshore events in the NE Caribbean. Solutions of A-quality have a FPU $< 25°$ and PROB $> 90\%$, B-quality have a FPU range within 25°–35° and PROB $> 80\%$, C-quality have a FPU range within 35°–45° and PROB $> 60\%$, and D-quality have a FPU range within 45°–75° and PROB $> 40\%$. Cumulatively, 22% of the focal mechanism solutions fall into the A, B, and C categories. From those, the data set was limited to events located within the area of concern and whose PROB was greater than 70%. The best constrained events were located within the OBS network where arrival observations included the *P* wave first-motion polarity and *S*/*P* amplitude ratio. Figure 2 shows an event (M_L1.7) plotted on a focal sphere with the first-motion polarities, *S*/*P* amplitude ratios, distribution of acceptable HASH-derived focal mechanism solutions, along with the A-quality preferred solution (an average of the acceptable solutions).

[15] To explore both lateral and depth dependence, the events were divided into 25 km depth intervals. Shallow events (0–10 km) generally had poorly constrained (D-quality) focal mechanism solutions, which likely resulted from hypocenters that were mislocated in depth; many had been located at the physically unrealistic 0 km focal depth. As shown by *Hardebeck and Shearer* [2002], depth errors will cause significant changes in computed takeoff angles for shallow events (<7 km). Only very few events were observed from 10 to 50 km and, of those, only D-quality solutions were produced. After removing D-quality events, the focii of the remaining events fell between 50 and 150 km depth. The remaining 76 fault plane solutions (Table S2 in the supporting information) were predominantly strike slip and oblique with several normal, reverse, and vertical mechanisms scattered through the study area.

[16] The primary region of interest, NE of Puerto Rico and centered between the five OBS instruments, was generally dominated by strike-slip focal mechanism solutions. The events are clustered in two different regions, one focused proximal to the islands and the other near 19.2°N, 64.5°W, which was also the location of the June swarm (Figure 1). Generally, the depth range 50–75 km showed the greatest concentration of strike-slip events in the region of the swarm, while the area near the islands contained both strike-slip and dip-slip events (Figure 3a). Events found within depths of 75–100 km also include a variety of strike- and dip-slip mechanisms, approximately half of which show a slight oblique combination of both (Figure 3b). Depths of 100–150 km showed an emergence of mechanisms dominated by oblique tension, which are discussed below (Figures 3c and 3d).

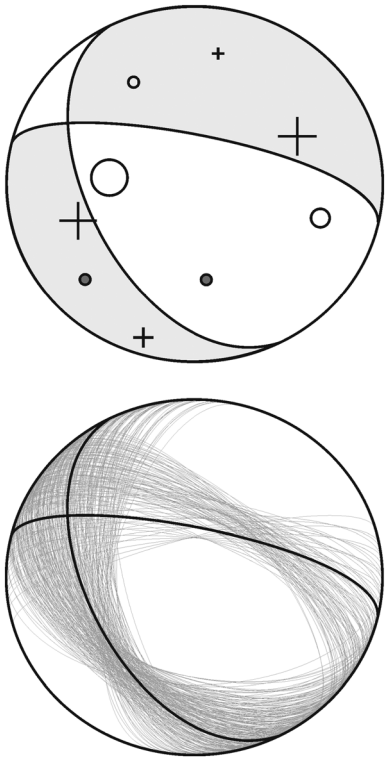

Figure 2. Focal mechanism solution from a M_L1.7 event, as derived from the HASH software. (top) Preferential solution of A-quality, found using both *P* wave first-motion polarities and *S*/*P* amplitude ratios. Locations of stations are denoted by symbols projected onto the focal sphere with their respective polarity observations: up, compressive (cross); down, dilatational (open circle); and no recorded ratio (filled circle). These symbols are scaled according to $\log_{10}$ *S*/*P* amplitude ratios, with larger symbols representing larger ratios. This event has a fault plane uncertainty of 23°, a 95% probability that the mechanism is close to the solution, and nine polarity observations, seven of which included ratio measurements. (bottom) Preferential focal mechanism solution (black curves) is plotted on top of the acceptable solutions (gray curves).

[17] The tensional axes of these focal mechanism solutions show a clear pattern, laterally and with depth (Figures 33a–3d). The majority of events located closer to the islands have tension axes oriented roughly N-S, perpendicular to the trench (Figures 3a–3d). Events farther to the northeast (near or within the June swarm region) have tension axes that are dominantly oriented NE-SW, with only a few exceptions (Figure 3a). This pattern of NE-SW tension continues at depths greater than 125 km; however, the number of these NE axes decreases with increasing depth. Within the depth interval of 100–125 km, the events have a mixed distribution of NE and NW oriented tension

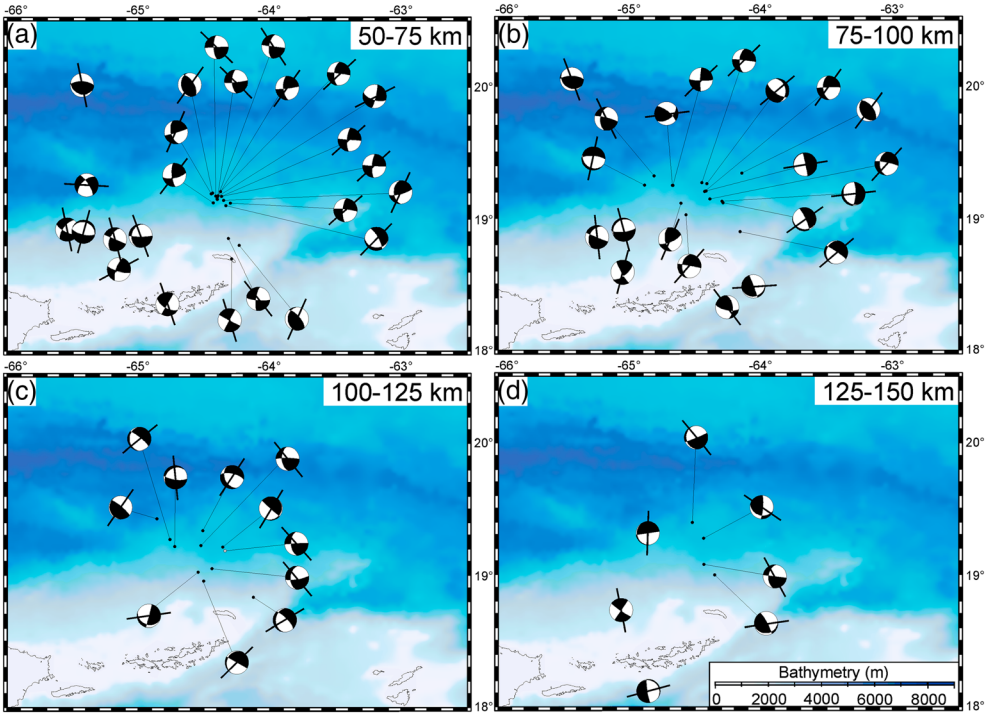

Figure 3. Bathymetric maps with focal mechanism solutions. The far eastern corner of Puerto Rico is seen in the bottom left of each subpart. The "beach ball" solutions are displayed in their corresponding ~25 km depth bin that is used throughout the data analysis, with the depth label in the top left corner of each subpart. Tensile stress axes are positioned on top of each beach ball. (a and b) Events near or within the June swarm region have tension axes dominantly oriented NE, with the southeast region of the map dominated by N-S tension. (c) Events are mainly contained to the swarm region and now incorporate a secondary tensile stress oriented NW. (d) The events at this depth mainly show tension oriented NW.

axes (Figure 3c). Then from 125 to 150 km, the tension axes offshore are primarily oriented NW (Figure 3d). The compression axes of the great majority of events in this segment at deeper depths (100–150 km) are oriented in the NE-SW direction, normal to the tension axes.

5. Stress Inversion

[18] In order to reveal spatial variations of the stress interactions and tectonic loading in the region, the stress field for our combined OBS-PRSN data set was computed using the damped inversion method of *Hardebeck and Michael* [2006]. To minimize the effects of errors associated with individual focal mechanisms, several inversion methods have been developed [*Abers and Gephart*, 2001; *Angelier*, 1984; *Gephart and Forsyth*, 1984; *Hardebeck and Michael*, 2006; *Horiuchi et al*., 1995; *Michael*, 1984, 1987, 1991]. Of these, the inversion method proposed by *Michael* [1984] is commonly used to determine the direction of the principal stress axes from focal mechanisms [e.g., *Imanishi et al*., 2011; *Matsumoto et al*., 2012; *Pasquale et al*., 2009; *Silva et al*., 2012; *Steffen et al*., 2012].

[19] Damped inversion methods aim to choose the best fit and least complex model from multiple permissible ones. Such a method was proposed by *Hardebeck and Michael* [2006], referred to as SATSI, which is an adaptive smoothing inversion that identifies variations required by the calculated focal mechanisms. The damping feature of SATSI finds a model by minimizing, in the least squares sense, the weighted sum of data misfit and model length. SATSI calculates the stress tensor that best fits a set of fault plane solutions using the standard linear inversion method of *Michael* [1984, 1987]. This results in the "least complex" stress tensor inversion model that fits the input focal mechanisms to within a user-specified acceptable level. Recent studies have shown that SATSI produces reliable stress tensors consistent with known structures and geology [*Steffen et al*., 2012; *Yoshida et al*., 2012].

[20] The region was gridded into equal 25 km × 25 km × 25 km subareas and each focal mechanism solution was assigned to its closest grid node. Following the methods of *Hardebeck and Michael* [2006], a spatial damping parameter of $e = 0.50$ was applied, as it minimized both the data variance and model length. The stress tensor results from all grid nodes were analyzed; tensile forces are summarized in Figure 4.

[21] Within the area of study, off the NE coast of Puerto Rico, the inversion was focused at depths of 50–150 km as this was the range with the largest number of well-constrained focal mechanism solutions. The inversion results have been grouped into two main stress regimes, SR1 and SR2; only the averaged vectors are shown in Figure 4. Through all four depth bins, the orientation of the tensile axes of SR1 was roughly N-S (Figure 4). The results from SR2 show a more complex interaction of tensile stress axes within the different depth slices. From

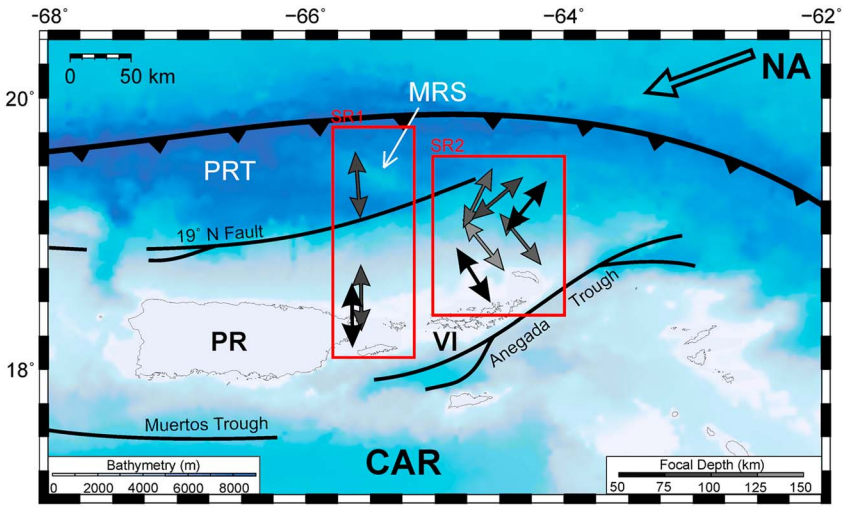

Figure 4. Bathymetric map showing a summary of the stress inversion results. Red boxes represent the study area and separate the two main stress fields. Arrows within the red boxes represent the dominant tensile stress vector for that area gray scaled according to their depth bin (dark, shallow; light, deep). The stress inversion results can be broken into two regions, SR1 and SR2. SR1 is dominated by N oriented tension with all depths. SR2 shows two main tensile stresses that span most depths. Shallower depths are dominated by NE tension while deeper bins are dominated by NW tension, with mixed stress directions in between. NA, North American Plate; CAR, Caribbean plate; PR, Puerto Rico; PRT, Puerto Rico Trench; MRS, Main Ridge Seamount.

50 to 100 km, the majority of tensile axes of SR2 were oriented NE-SW (Figure 4). From 100 to 125 km, SR2 shows a combination of NE and NW trending tensile forces as determined from the stress inversion. The deepest bin, 125–150 km, shows inversion results dominated by NW-SE oriented tension axes (Figure 4).

6. Discussion

[22] Two major stress regimes are generated by flexural bending of a subducting slab as it enters a trench: (1) a shallow regime where the slab is undergoing extension parallel to the subduction direction, generating shallow trench-normal tensional stress axes; and (2) a deep regime where the slab is being compressed as it bends downdip, generating deep trench-normal compressive stresses [*Bautista et al*., 2001]. This combination of depth-dependant compressional and tensional stresses caused by flexural bending can occur with the subduction phenomenon of slab rollback, caused by trench-parallel mantle flow [*Buttles and Olson*, 1998; *Civello and Margheriti*, 2004; *Kincaid and Griffiths*, 2003; *Kneller and van Keken*, 2007].

[23] The oblique subduction along the curved convergent margin produced a variety of earthquake mechanism types, which transition from primarily pure dip slip and strike slip to more oblique with an increase in depth (Figure 3). Regardless of faulting style, the majority of our study area is characterized by NE-SW oriented stress inversion tensile axes, which are consistent with oblique convergence of the NOAM and CAR plates along the Puerto Rico Trench [*Calais et al*., 2002; *DeMets et al*., 2010; *Jansma et al*., 2000; *Mann et al*., 2002]. Shallow depths along the Puerto Rico Trench are where compressional axes of the Wadati-Benioff zone are oriented parallel to the trench (perpendicular to the trench-normal tension; see Figure 3). This is a pattern documented in other regions, such as Sumatra and Java [*Slancova et al*., 2000], and is likely due to subduction zone curvature and subsequent lateral stresses.

[24] The N-S oriented tensile stress field in SR1 coincides with an extensional regime dominated by flexural bending of the NOAM lithosphere. This region west of 65°W demonstrates a single uniform stress direction with only limited depth coverage. In contrast, the tensile stress field of SR2 (east of 65°W) has a combination of both trench-normal extension (at shallow depths) with trench-normal compression (at greater depths), indicative of flexural bending of downgoing lithosphere at the point of entry into the subduction trench, and is likely controlled by slab rollback, trench-parallel mantle flow, and, perhaps, trench-normal mantle flow. Figure 5 shows a schematic of the local tectonics with associated stress fields and mantle flow directions.

[25] Mantle flow generally parallels the plate boundaries of the Caribbean and slab rollback is the mechanism commonly attributed to this pattern [*Meighan and Pulliam*, 2013; *Piñero-Feliciangeli and Kendall*, 2008; *Russo et al*., 1996; *Russo and Silver*, 1994]. Shear wave splitting measurements of seismic anisotropy indicate this trench-parallel mantle flow direction. However, a recent study of seismic anisotropy in the NE Caribbean suggests that the mantle also flows through a gap in the NOAM slab, at approximately 65°W, where the direction of fast polarization was found to be oriented perpendicular to the trench (see mantle flow arrows in Figure 5) [*Meighan and Pulliam*, 2013]. The explanation proposed here is also consistent with recent evidence that supports the existence of a slab tear from *ten Brink and López-Venegas* [2012], in which these authors interpret NW motion, as determined by continuous GPS observations, as a result of a tear.

[26] The data suggest that the proposed tear is located between the two distinct stress regimes, SR1 and SR2,

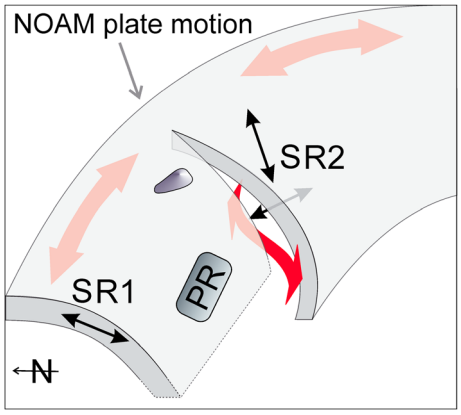

Figure 5. Curved subduction zone and stress field schematic. This tectonic regime is one of oblique convergence at the corner of the plate boundary, with a proposed tear to accommodate such geometry that requires crustal shortening, extension, and shearing. The stress inversion summary vectors (black arrows) have been included on the model sketch to show the relative location of the tension axes within the slab, vertically and laterally. SR1 is dominated by N-S tension, which is likely due to downdip crustal extension of the NOAM slab west of the tear. SR2 has two stress field components: The shallow tensile stress field is oriented parallel to plate motion, corresponding to lithospheric flexural extension of the downgoing slab; the deep tensile stress field oriented trench-parallel is related to lithospheric flexural compression that occurs at depth. The red arrows represent likely mantle flow patterns as suggested by *Meighan and Pulliam* [2013] to flow behind the intact slab (trench-parallel) and through the slab gap created by a tear (trench-normal). The dashed line at the base of the NOAM slab indicates a possible detached slab. NOAM, North American Plate; PR, Puerto Rico; SR1 and SR2, stress regimes 1 and 2. Tensile stress direction (black arrows); mantle flow direction (red arrows); Main Ridge Seamount (blue object).

creating two segments of the NOAM slab at approximately longitude 65°W. It is here where a significant shift in trench morphology was observed and determined to be caused by the collapse of the Puerto Rico Trench at 3.3 Ma [*ten Brink*, 2005]. Seafloor morphology features west of 65°W include a wider trench that is deeper and plunges more steeply into the mantle than that of the trench segment east of 65°W [*ten Brink*, 2005]. This is also the location at which the Puerto Rico Trench curves most sharply and is thus subjected to increased lateral strain [*Toda and Stein*, 2002; *ten Brink*, 2005].

[27] The results of this study, as well as the studies cited above, are consistent with a scenario in which the Main Ridge Seamount serves as an impediment to NOAM subduction. Main Ridge is a 50 km long, 2 km high aseismic volcanic ridge being subducted at the Puerto Rico Trench, as interpreted by *ten Brink* [2005] and *McCann and Sykes* [1984] (Figure 4). Sandbox models of seamount subduction [*Dominguez et al*., 2000] predict the formation of strike-slip faults where the seamount has entered the trench. A northeast trending strike-slip fault has since been observed and mapped off the eastern edge of the seamount by *ten Brink* [2005]. In this scenario, westward motion of the NOAM slab continues south of this fault, likely demarcated by the swarms and associated events recorded by the OBS deployment. A seamount is expected to generate resistance to subduction [*Gutscher et al*., 1999] and stress modeling calculations have confirmed that large tensile stresses develop within the slab downdip of a seamount [*Toda and Stein*, 2002; *ten Brink*, 2005]. *ten Brink* [2005] proposed that the onset of Main Ridge Seamount subduction was the proximate cause of the tear and the point of continued rupture propagation is represented by the locus of the swarms. Stress field results support that interpretation indirectly, in that a significant change in the state of stress is revealed by earthquakes from west to east but this change cannot be attributed directly to tearing. Rather, the stress regime in the eastern slab segment (SR2) suggests that the slab is undergoing rollback while the segment immediately to the west is not. These two regimes in such close proximity are incompatible in a single, intact slab. A simpler interpretation is that the lithosphere that entered the subduction zone as a single slab has separated into two and that each of the two stress patterns represents the state of stress in a distinct portion of the former slab. Whether the swarms recorded by OBS represent the propagating tear is unclear; an explanation would have to be found that explains their occurrence over a depth range of 50–150 km and their separation into two distinct stress patterns that correspond to distinct focal depth ranges (50–100 km and 100–150 km). The more easily supportable and straightforward interpretation is that the two stress patterns (SR1 and SR2) represent separate slabs that are experiencing different stresses. A preponderance of evidence accumulated by a variety of studies, including this one, supports the conclusion that a slab tear must exist between SR1 and SR2 in Figure 5.

7. Conclusions

[28] The nature of oblique, curved subduction zones is one that requires, at various locations along its strike, crustal shortening, extension, and shearing in order to accommodate the subduction zone's complex geometry [*Bautista et al*., 2001]. When evaluated in the context of previous studies, these results ultimately support the hypothesis that the subducting NOAM plate is tearing in the NE corner of the CAR plate boundary. A tear would allow the NOAM slab to negotiate the sharp turn at the NE Caribbean plate boundary and accounts for the GPS, gravity, morphological, and seismic anisotropy observations reported by previous authors [*ten Brink and López-Venegas*, 2012; *ten Brink*, 2005; *Meighan and Pulliam*, 2013], in addition to these focal mechanism solutions and stress inversion modeling. The actively increasing rate of seismicity and the location of swarms suggest that the tear is still propagating. In this study, a tear in the NOAM slab is supported by the discovery of two distinct stress regimes: SR2 (east of the tear) is likely dominated by slab rollback and SR1 (west of the tear) has a consistent stress pattern that is coherent with downdip extension. Slab tearing is the likely mechanism that isolates these stress regimes and allows the slab segments to respond quite differently over a short distance. The small number of deep events located north of Puerto Rico, within SR1, further suggests the possibility of slab detachment in that region. Additional observations are needed before the connection between the downdip extensional stress regime, the extreme low gravity

anomaly, and seismicity in this region and their connection to the slab tear can be understood fully.

[29] **Acknowledgments.** We thank Victor A. Huérfano, Alan Gunnell, Ben Skrabanek, and staffs of the Puerto Rico, IRIS/USGS, and Netherlands Antilles seismic networks for waveform data and the U.S. National Ocean Bottom Seismic Instrumentation Pool at the Woods Hole Oceanographic Institute for OBS services. We also give special thanks to the Associate Editor, Robert Nowack, two anonymous reviewers, and Danielle Sumy for their thorough and constructive comments. HEM also appreciates discussions with John Dunbar, Vince Cronin, Jeanne Hardebeck, and Björn Lund. Seismic waveform data recorded by the OBS are archived at the IRIS Data Management Center.

References

Abers, G. A., and J. W. Gephart (2001), Direct inversion of earthquake first motions for both the stress tensor and focal mechanisms and application to southern California, *J. Geophys. Res.*, *106*(B11), 26,523–26,540, doi:10.1029/2001JB000437.

Angelier, J. (1984), Tectonic analysis of fault slip data set, *J. Geophys. Res.*, *89*, 5835–5848.

Barberi, G., L. Beranzoli, P. Favali, G. Neri, and T. Sgroi (2006), Seismic location improvements from an OBS/H temporary network in southern Tyrrhenian Sea, *Ann. Geophys*, *49*(2–3), 739–749.

Bautista, B. C., M. L. P. Bautista, K. Oike, F. T. Wu, and R. S. Punongbayan (2001), A new insight on the geometry of subducting slabs in northern Luzon, Philippines, *Tectonophysics*, *339*, 279–310.

Begnaud, M. L., K. C. McNally, D. S. Stakes, and V. A. Gallardo (2000), A crustal velocity model for locating earthquakes in Monterey Bay, California, *Bull. Seismol. Soc. Am.*, *90*(6), 1391–1408.

Boese, C. M., J. Townend, E. Smith, and T. Stern (2012), Microseismicity and stress in the vicinity of the Alpine Fault, central Southern Alps, New Zealand, *J. Geophys. Res.*, *117*, B02302, doi:10.1029/2011JB008460.

ten Brink, U. (2005), Vertical motions of the Puerto Rico Trench and Puerto Rico and their cause, *J. Geophys. Res.*, *110*, B06404, doi:10.1029/2004JB003459.

ten Brink, U. S., and A. M. López-Venegas (2012), Plate interaction in the NE Caribbean subduction zone from continuous GPS observations, *Geophys. Res. Lett.*, *39*, L10304, doi:10.1029/2012GL051485.

Buttles, J., and P. Olson (1998), A laboratory model of subduction zone anisotropy, *Earth Planet. Sci. Lett.*, *164*, 245–262, doi:10.1016/S0012-821X(98)00211-8.

Calais, E., Y. Mazabraud, P. Mercier de Lepinay, P. Mann, G. S. Mattioli, and P. E. Jansma (2002), Strain partitioning and fault slip rates in the northeastern Caribbean from GPS measurements, *Geophys. Res. Lett.*, *29*(18), 1856, doi:10.1029/2002GL015397.

Chang, E. T. Y., S.-K. Hsu, and C.-S. Lee (2008), Earthquake swarm recorded by an ocean bottom seismic array in Southwest offshore of Taiwan in October, 2005, *Terr. Atmos. Ocean. Sci.*, *19*(6), 717–728.

Civello, S., and L. Margheriti (2004), Toroidal mantle flow around the Calabrian slab (Italy) from SKS splitting, *Geophys. Res. Lett.*, *31*, L10601, doi:10.1029/2004GL019607.

Clark, S. A., M. Sobiesiak, C. A. Zelt, M. B. Magnani, M. S. Miller, M. J. Bezada, and A. Levander (2008), Identification and tectonic implications of a tear in the South America plate at the southern end of the Lesser Antilles, *Geochem. Geophys. Geosyst.*, *9*, Q11004, doi:10.1029/2008GC002084.

Clinton, J. F., G. Cua, V. Huérfano, C. von Hillebrandt-Andrade, and J. Martinez Cruzado (2006), The current state of seismic monitoring in Puerto Rico, *Seismol. Res. Lett.*, *77*(5), 532–543.

Coudert, E., B. L. Isacks, M. Barazangi, R. Louat, R. Cardwell, A. Chen, J. Dubois, G. Latham, and B. Pontoise (1981), Spatial distribution and mechanisms of earthquakes in the southern New Hebrides arc from a temporary land and ocean bottom seismic network and from worldwide observations, *J. Geophys. Res.*, *86*, 5905–5925.

Dahm, T. (2006), Seismic broadband ocean-bottom data and noise observed with free-fall stations: Experiences from long-term deployments in the North Atlantic and the Tyrrhenian Sea, *Bull. Seismol. Soc. Am.*, *96*(2), 647–664, doi:10.1785/0120040064.

DeMets, C., R. G. Gordon, and D. F. Argus (2010), Geologically current plate motions, *Geophys. J. Int.*, *181*, 1–80.

Dominguez, S., J. Malavieille, and S. E. Lallemand (2000), Deformation of accretionary wedges in response to seamount subduction: Insights from sandbox experiments, *Tectonics*, *19*, 182–196.

Engdahl, E. R., R. D. van der Hilst, and R. P. Buland (1998), Global teleseismic earthquake relocation with improved travel times and procedures for depth determination, *Bull. Seismol. Soc. Am.*, *88*, 722–743.

Fischer, K., and W. McCann (1984), Velocity modeling and earthquake relocation in the northeast Caribbean, *Bull. Seismol. Soc. Am.*, *74*(4), 1249–1262.

Frohlich, C., S. Billington, E. R. Engdahl, and A. Malahoff (1982), Detection and location of earthquakes in the central Aleutian subduction zone using island and ocean bottom seismograph stations, *J. Geophys. Res.*, *87*, 6853–6864.

Gephart, J. W., and D. W. Forsyth (1984), An improved method for determining the regional stress tensor using earthquake focal mechanism data: Application to the San Fernando earthquake sequence, *J. Geophys. Res.*, *89*, 9305–9320.

Govers, R., and M. J. R. Wortel (2005), Lithosphere tearing at STEP faults: Response to edges of subduction zones, *Earth Planet. Sci. Lett.*, *236*(1–2), 505–523, doi:10.1016/j.epsl.2005.03.022.

Gutscher, A., J. Malavieille, S. Lallemand, and J. Y. Collot (1999), Tectonic segmentation of the North Andean margin: Impact of the Carnegie Ridge collision, *Earth Planet. Sci. Lett.*, *168*, 255–270.

Hardebeck, J. L., and A. J. Michael (2006), Damped regional-scale stress inversions: Methodology and examples for southern California and the Coalinga aftershock sequence, *J. Geophys. Res.*, *111*, B11310, doi:10.1029/2005JB004144.

Hardebeck, J. L., and P. M. Shearer (2002), A new method for determining first-motion focal mechanisms, *Bull. Seismol. Soc. Am.*, *92*(6), 2264–2276.

Hardebeck, J. L., and P. M. Shearer (2003), Using *S*/*P* amplitude ratios to constrain the focal mechanisms of small earthquakes, *Bull. Seismol. Soc. Am.*, *93*(6), 2434–2444.

Horiuchi, S., G. Rocco, and A. Hasegawa (1995), Discrimination of fault planes from auxiliary planes based on simultaneous determination of stress tensor and a large number of fault plane solutions, *J. Geophys. Res.*, *100*, 8327–8338, doi:10.1029/94JB03284.

Imanishi, K., Y. Kuwahara, T. Takeda, T. Mizuno, H. Ito, K. Ito, H. Wada, and Y. Haryu (2011), Depth-dependent stress field in and around the Atotsugawa fault, central Japan, deduced from microearthquake focal mechanisms: Evidence for localized aseismic deformation in the downward extension of the fault, *J. Geophys. Res.*, *116*, B01305, doi:10.1029/2010JB007900.

Jansma, P. E., G. S. Mattioli, A. López-Venegas, C. DeMets, T. H. Dixon, P. Mann, and E. Calais (2000), Neotectonics of Puerto Rico and the Virgin Islands, northeastern Caribbean, from GPS geodesy, *Tectonics*, *19*(6), 1021–1037, doi:10.1029/1999TC001170.

Julian, B. R., and G. R. Foulger (1996), Earthquake mechanisms from linear programming inversion of seismic-wave amplitude ratios, *Bull. Seismol. Soc. Am.*, *86*, 972–980.

Kennett, B. L. N., and E. R. Engdahl (1991), Traveltimes for global earthquake location and phase identification, *Geophys. J. Int.*, *105*, 429–465.

Kilb, D., and J. L. Hardebeck (2006), Fault parameter constraints using relocated earthquakes: A validation of first-motion focal-mechanism data, *Bull. Seismol. Soc. Am.*, *96*(3), 1140–1158, doi:10.1785/0120040239.

Kincaid, C., and R. W. Griffiths (2003), Laboratory models of the thermal evolution of the mantle during rollback subduction, *Nature*, *425*, 58–62, doi:10.1038/nature01923.

Kisslinger, C. (1980), Evaluation of *S* to *P* amplitude ratios for determining focal mechanisms from regional network observations, *Bull. Seismol. Soc. Am.*, *70*, 999–1014.

Kneller, E. A., and P. E. van Keken (2007), Trench-parallel flow and seismic anisotropy in the Mariana and Andean subduction systems, *Nature*, *450*, 1222–1225, doi:10.1038/nature06429.

Kraft, T., J. Wassermann, and H. Igel (2006), High-precision relocation and focal mechanism of the 2002 rain-triggered earthquake swarms at Mt. Hochstaufen, SE Germany, *Geophys. J. Int.*, *167*, 1513–1528, doi:10.1111/j.1365-246X.2006.03171.

Lomax, A., J. Virieux, P. Volant, and C. Berge (2000), Probabilistic earthquake location in 3D and layered models: Introduction of a Metropolis-Gibbs method and comparison with linear locations, in *Advances in Seismic Event Location*, edited by C. H. Thurber and N. Rabinowitzm, pp. 101–134, Kluwer, Amsterdam.

López, A., J. Pulliam, U. ten Brink, H. E. Mintz, and C. von Hillebrandt-Andrade (2009), Deployment of ocean bottom seismometers south of Puerto Rico Trench yields new insights into the behavior of seismic swarms, *Eos Trans. AGU*, *90*(52), Fall Meet. Suppl., Abstract T23B-1902.

Mann, P., E. Calais, J.-C. Ruegg, C. DeMets, P. E. Jansma, and G. S. Mattioli (2002), Oblique collision in the northeastern Caribbean from GPS measurements and geological observations, *Tectonics*, *21*(6), doi:10.1029/2001TC001304.

Matsumoto, S., K. Uehira, T. Matsushima, and H. Shimizu (2012), Modeling heterogeneous deviatoric stress field around the hypocentral area of the 2005 Fukuoka earthquake (*M*7.0) by spatially distributed moment tensors, *J. Geophys. Res.*, *117*, B03303, doi:10.1029/2011JB008687.

Maurice, S. D. R., D. A. Wiens, P. J. Shore, E. Vera, and L. M. Dorman (2003), Seismicity and tectonics of the South Shetland Islands and Bransfield Strait from a regional broadband seismograph deployment, *J. Geophys. Res.*, *108*(B10), 2461, doi:10.1029/2003JB002416.

McCann, W. L., and L. R. Sykes (1984), Subduction of aseismic ridges beneath the Caribbean Plate: Implications for the tectonics and seismic potential of the northeastern Caribbean, *J. Geophys. Res.*, *89*, 4493–4519.

Meighan, H. E., and J. Pulliam (2013), Seismic anisotropy beneath the Northeastern Caribbean: Implications for the subducting North American lithosphere, in *Caribbean Geosciences*, edited by O. Lacombe, J.F. Lebrun and B. *Marcaillou, Bull. Soc. Geol. Fr.*, *184*(1), 69–79.

Michael, A. J. (1984), Determination of stress from slip data: Faults and Folds, *J. Geophys. Res.*, *89*, 11,517–11,526.

Michael, A. J. (1987), Use of focal mechanisms to determine stress: A control study, *J. Geophys. Res.*, *92*, 357–368, doi:10.1029/JB092iB01p00357.

Michael, A. J. (1991), Spatial variations in stress within the 1987 Whittier Narrows, California, aftershock sequence: New techniques and results, *J. Geophys. Res.*, *96*, 6303–6319, doi:10.1029/91JB00195.

Millen, D. W., and M. W. Hamburger (1998), Seismological evidence for tearing of the Pacific plate at the northern termination of the Tonga subduction zone, *Geology*, *26*(7), 659–662.

Miller, M. S., A. Gorbatov, and B. L. Kennett (2006), Three-dimensional visualization of a near-vertical slab tear beneath the southern Mariana arc, *Geochem. Geophys. Geosyst.*, *7*, Q06012, doi:10.1029/2005GC001110.

Montagner, J. et al. (1994), The French pilot experiment OFM-SIS-MOBS: First scientific results on noise level and event detection, *Phys. Earth Planet. Inter.*, *84*, 321–336.

Moser, T. J., T. van Eck, and G. Nolet (1992), Hypocenter determination in strongly heterogeneous earth models using the shortest path method, *J. Geophys. Res.*, *97*, 6563–6572.

Nishizawa, A., T. Kanazawa, T. Iwasaki, and H. Shimamura (1992), Spatial distribution of earthquakes associated with the Pacific plate subduction off northeastern Japan revealed by ocean bottom and land observation, *Phys. Earth Planet. Inter.*, *75*(1–3), 165–175.

Pasquale, G., R. De Matteis, A. Romeo, and R. Maresca (2009), Earthquake focal mechanisms and stress inversion in the Irpinia region (southern Italy), *J. Seismol.*, *13*, 107–124.

Piñero-Feliciangeli, L. T., and J. -M. Kendall (2008), Sub-slab mantle flow parallel to the Caribbean plate boundaries: Inferences from SKS splitting, *Tectonophysics*, *462*, 22–34.

Pontoise, B., and T. Monfret (2004), Shallow seismogenic zone detected from an offshore-onshore temporary seismic network in the Esmeraldas area (northern Ecuador), *Geochem. Geophys. Geosyst.*, *5*, Q02009, doi:10.1029/2003GC000561.

Pulliam, J., Y. Nakamura, C. Huerto-Lopez, and B. Yates (2003), Field test of an inexpensive, small broadband ocean-bottom seismograph, *Bull. Seismol. Soc. Am.*, *93*(1), 152–171.

Pulliam, J., V. A. Huérfano, U. ten Brink, and C. von Hillebrandt-Andrade (2007), Seismic sequences in the Sombrero Seismic Zone, *Eos. Trans. AGU*, *88*(23), Jt. Assem. Suppl., Abstract S52A-02.

Roland, E., and J. J. McGuire (2009), Earthquake swarms on transform faults, *Geophys. J. Int.*, *178*, 1677–1690.

Rosenbaum, G., M. Gasparon, F. P. Lucente, A. Peccerillo, and M. S. Miller (2008), Kinematics of slab tear faults during subduction segmentation and implications for Italian magmatism, *Tectonics*, *27*, TC2008, doi:10.1029/2007TC002143.

Russo, R., and P. G. Silver (1994), Trench-parallel flow beneath the Nazca Plate from seismic anisotropy, *Science*, *263*, 1105–1111.

Russo, R. M., P. G. Silver, M. Franke, W. B. Ambeh, and D. E. James (1996), Shear-wave splitting in northeast Venezuela, Trinidad, and the eastern Caribbean, *Phys. Earth Planet. Inter.*, *95*, 251–275.

Shen, Y., D. W. Forsyth, J. Conder, and L. M. Dorman (1997), Investigation of microearthquake activity following an intraplate teleseismic swarm on the west flank of the southern East Pacific Rise, *J. Geophys. Res.*, *102*, 459–475.

Silva, R., J. Havskov, C. Bean, and N. Wallenstein (2012), Seismic swarms, fault plane solutions, and stress tensors for São Miguel Island central region (Azores), *J. Seismol.*, *16*(3), 389–407, doi:10.1007/s10950-012-9275-x.

Slancova, A., A. Spicak, and J. Vanek (2000), How the state of stress varies in the Wadati-Benioff zone: Indications from focal mechanisms in the Wadati-Benioff zone beneath Sumatra and Java, *Geophys. J. Int.*, *143*, 909–930.

Snoke, J. A., J. W. Munsay, A. G. Teague, and G. A. Bollinger (1984), A program for focal mechanism determination by combined use of polarity and SV-P amplitude ratio data, *Earth Notes*, *55*(3), 15.

Sørensen, M. B., P. H. Voss, J. Havskov, S. Gregersen, and K. Atakan (2011), The seismotectonics of western Skagerrak, *J. Seismol.*, *15*(4), 599–611, doi:10.1007/s10950-011-9235-x.

Steffen, R., D. W. Eaton, and P. Wu (2012), Moment tensors, state of stress and their relation to post-glacial rebound in northeastern Canada, *Geophys. J. Int.*, *189*(3), 1741–1752, doi:10.1111/j.1365-246X.2012.05452.x.

Tarantola, A., and B. Valette (1982), Generalized nonlinear inverse problems solved using the least squares criterion, *Rev. Geophys. Space Phys.*, *20*, 219–232.

Toda, S., and R. S. Stein (2002), Response of the San Andreas fault to the 1983 Coalinga-Nuñez earthquakes: An application of interaction-based probabilities for Parkfield, *J. Geophys. Res.*, *107*(B6), 2126, doi:10.1029/2001JB000172.

Webb, S. C. (1998), Broadband seismology and noise under the ocean, *Rev. Geophys.*, *36*, 105–142.

Wittlinger, G., G. Herquel, and T. Nakache (1993), Earthquake location in strongly heterogeneous media, *Geophys. J. Int.*, *115*, 759–777.

Yang, W., E. Hauksson, and P. M. Shearer (2012), Computing a large refined catalog of focal mechanisms for Southern California (1981–2010): Temporal stability of the style of faulting, *Bull. Seismol. Soc. Am.*, *102*(3), 1179–1194, doi:10.1785/0120110311.

Yoshida, K., A. Hasegawa, T. Okada, T. Iinuma, Y. Ito, and Y. Asano (2012), Stress before and after the 2011 great Tohoku-oki earthquake and induced earthquakes in inland areas of eastern Japan, *Geophys. Res. Lett.*, *39*, L03302, doi:10.1029/2011GL049729.